Heat Treatment Influence on the Corrosion Resistance of a Cu-Al-Fe-Mn Bronze

MARIANA CIURDAS[1], IOANA ARINA GHERGHESCU[2]*, SORIN CIUCA[2], ALINA DANIELA NECSULESCU[2], COSMIN COTRUT[2], RUXANDRA ELENA DUMITRESCU[2]*

[1] Politehnica University of Bucharest, Materials Science and Engineering Faculty, Department of Engineering and Management of Metallic Materials Production, 313 Splaiul Independentei, 060042 Bucharest, Romania

[2] Politehnica University of Bucharest, Materials Science and Engineering Faculty, Department of Materials Science and Physical Metallurgy, 313 Splaiul Independentei, 060042 Bucharest, Romania

Aluminium bronzes are exhibiting good corrosion resistance in saline environments combined with high mechanical properties. Their corrosion resistance is obviously confered by the alloy chemical composition, but it can also be improved by heat treatment structural changes. In the present paper, five Cu-Al-Fe-Mn bronze samples were subjected to annealing heat treatments with furnace cooling, water quenching and water quenching followed by tempering at three different temperatures: 200, 400 and 550°C. The heating temperature on annealing and quenching was 900°C. The structure of the heat treated samples was studied by optical and scanning electron microscopy. Subsequently, the five samples were submitted to corrosion tests. The best resistance to galvanic corrosion was showed by the quenched sample, but it can be said that all samples are characterized by close values of open-circuit potentials and corrosion potentials. Concerning the susceptibility to other types of corrosion (selective leaching, pitting, crevice corrosion), the best corrosion resistant structure consists of α solid solution, γ_2 and k compounds, corresponding to the quenched and 550°C tempered sample.

Keywords: Cu-Al-Fe-Mn bronze, corrosion resistance, heat treatments

Aluminium bronze combines excellent corrosion resistance especially in seawater with high mechanical properties. These features makes them proper to be used mainly in shipbuilding applications such as sea cocks, pumps, bushes, bearings, shafts, propellers etc.

The remarkable corrosion resistance is determined by the presence of 8 to 12% aluminium which, along with copper, promotes the formation of a thin, adherent, compact and self-regenerating oxide layer [1-3]. An improvement of chemical and mechanical properties can be achieved by adding nickel, iron and manganese. As far as the influence on corrosion resistance is concerned, these chemical elements contribute to the suppression of the γ_2 phase resulting from the eutectoid transformation of β-phase found in the Cu-Al binary system [4]. Thus, instead of the Cu_9Al_4 intermetallic compound, whose formation implies a decrease in the aluminium content of the solid solution and thereby a decrease in corrosion resistance, k phases are found in the structure. The latter show a variable composition in nickel, iron and aluminium, being classified as follows [5, 6]:

k_I - primary compound Fe_3Al obtained directly from the melt in bronzes with an iron content of over 5%;

k_{II} - Fe_3Al secondary compound formed by precipitation in β phase at high temperatures ranging between 900 and 950°C;

k_{III} - NiAl compound precipitating in conjunction with α phase as a result of the eutectoid decomposition of β phase;

k_{IV} - similar to k_{II}, formed by precipitation in α phase at lower temperatures;

k_V - similar to k_{III}, formed during the β phase decomposition on heating (upon tempering).

Regarding the mechanical characteristics, all alloying elements are increasing the resistance; aluminium has the largest contribution, followed by manganese (in this respect, a percentage of aluminium equals six percentages of manganese), nickel and iron.

Both the corrosion resistance and the mechanical strength properties of these bronzes are structurally dependent and can be improved by specific heat treatments.

Aluminium bronze with iron and manganese additions are a cheaper version of nickel bronze (NAB) and are also characterized by good corrosion resistance and high mechanical properties.

Experimental part

The object of the present research is a bronze with aluminium, iron and manganese. The chemical composition determined by optical emission spectromery on a SPECTROMAXx M apparatus is given in table 1. Samples were cut from a 50 mm diameter bar, obtained by continuous casting.

Five cylindrical samples with a height of 40 mm were drilled from the bar and each sample was then longitudinally sectioned in four, along perpendicular diameters. The 20 samples were heat treated in a Nabertherm furnace (volume 3l, inner dimensions WxDxH: 160x140x100 mm, maximum heating temperature 1100°C). The heat treatments are shown in table 2.

Five heat treated samples, codified by B1, B2, B3, B4 and B5, were selected for investigation by optical and

Chemical element	Cu	Al	Fe	Mn	Pb	Ni	Zn	Sn
%	87.16	10.20	1.32	1.21	0.061	0.020	0.018	0.011

Table 1
THE CHEMICAL COMPOSITION OF THE Cu-Al-Fe-Mn BRONZE

* email: gherghescu_ioana@yahoo.com; ruxandraelenadumitrescu@gmail.com; Phone: (+40)723344813

Sample Code / Number of samples	Heat treatment	Heat treatment parameters
B1/4	Annealing	900°C/1h/furnace cooling
B2/4	Quenching	900°C/1h/water cooling
B3/4	Quenching + tempering	900°C/1h/water cooling + 200°C/2h/air cooling
B4/4	Quenching + tempering	900°C/1h/water cooling + 400°C/2h/air cooling
B5/4	Quenching + tempering	900°C/1h/water cooling + 550°C/2h/air cooling

Table 2
HEAT TREATMENTS APPLIED TO CU-AL-Fe-Mn BRONZE SAMPLE

electronic microscopy techniques. Another set of five samples codified by B1, B2, B3, B4 and B5 was evaluated for corrosion resistance by the linear polarization resistance technique.

The corrosion resistance evaluation tests were performed using a Potentiostat/Galvanostat (PARSTAT 4000 model, Princeton Applied Research), and potentiodynamic polarization curves were acquired using the VersaStudio v 2.50.3 software.

In order to perform the tests an electrochemical cell was used, consisting of a calomel saturated electrode (SCE) as a reference electrode, a platinum electrode as a recording electrode and the working electrode consisting of the investigated samples.

The tests were performed in 3.5% NaCl saline solution at 25°C. Before performing them, the samples were immersed in the electrolyte until the open circuit potential stabilization (OCP) was established.

Along these tests, the following parameters were determined:

- Open circuit potential after 6 h (E_{oc})
- Corrosion potential (E_{corr})
- Corrosion current density (i_{corr})
- The cathodic curve slope (β_c),
- The anodic curve slope (β_a).

With the help of the parameters determined by the Tafel technique, the polarization resistance was also calculated; the latter is needed to characterize the corrosion resistance.

The polarization resistance was performed according to ASTM G59-97 (2003) using the equation:

$$R_p = \frac{1}{2.3} \cdot \frac{\beta_a \beta_c}{\beta_a + \beta_c} \cdot \frac{1}{i_{corr}} \quad (1)$$

where:

R_p - the polarization resistance, kΩxcm^2
β_a - the anodic curve slope,
β_c - the cathodic curve slope,
i_{corr} – the corrosion current density, μA/cm^2

The calculation of the corrosion rate was performed according to ASTM G102-89 (2004) using the formula:

$$CR = K_i \frac{i_{corr}}{\rho} EW \quad (2)$$

where: CR - is the corrosion rate, mm/y
K_i - 3.27x10^{-3} mm×g/μA/cm/y
ρ - the alloy density, g/cm^3
i_{corr} - the corrosion current density, μA/cm^2
EW - the equivalent weight (dimensionless)

Results and discussions

Optical and scanning electron microscopy

The optical and scanning electron microscopy microstructures of B1-B5 samples are shown in figures 1-5.

The microstructure of sample B1 (fig.1) consists of light coloured rod-like crystals of solid proeutectoid solution α, of iron-rich precipitated phases (phases k**)**, of eutectoid mechanical mixture consisting of α and γ_2 (possibly also k_{III}) as well as low amounts of metastable phases α*****: martensite (α'_1) and bainite (α_B) [4].

Although the cooling on annealing was performed slowly with the furnace and the constituents should have been exclusively equilibrium ones, both optical and scanning electron micrographs revealed the presence of a mixture of out-of-equilibrium phases, α*****.

Thus, light coloured plate-like crystals of α_B, intersected at obtuse angles, distributed at the boundaries of the proeutectoid phase crystals, along with dark areas (martensite + eutectoid), are observed.

The mixture α*****(α'_1 + α_B) is therefore formed also at relatively low cooling rates, as confirmed by the TRC curves [3], drawn for a 10.5% Al bronze.

The existence of the mixture α***** in the structure is explained by the small size of the samples, which imparts an accelerated cooling rate, even on furnace cooling.

Regarding the influence of Fe on the Cu-Al-Fe-Mn bronze microstructure, the concentration of about 1.5% Fe results in the precipitation of an iron-rich phase (k_{II}) in the β phase, with no apparent tendencies of location on grain boundaries [7].

Thus gray-blue coloured rosette-like precipitates k_{II} can be seen in figure 1a, distributed within the proeutectoid phase grains as well as in α* and the eutectoid mixture.

The k_{IV} phase, in the form of very fine high-dispersion precipitations, can only be seen inside the rod-like proeutectoid solid solution crystals.

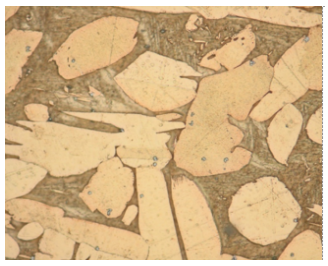

Fig. 1.a) Optical microstructure of B1 sample, x 500; reagent: 25mL HCl + 5g $FeCl_3$ + 100mL H_2O

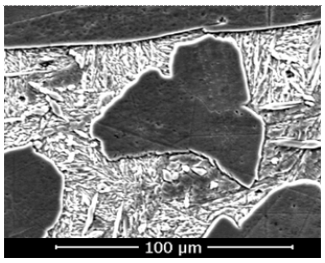

Fig. 1.b) Scanning electron micrograph of B1 sample, secondary electron image α solid solution (black crystals), plate-like α_B (light zones) and eutectoid + martensite (gray and dark-gray zones between light bainite microvolumes)

The microstructure of B2 sample shown in figure 2 reveals a mixed structure of martensite (the dark areas in fig. 1a, fig. 3b) and light coloured platiform bainite (α solid solution, Widmanstatten-like, with some degree of oversaturation, obtained by massive transformation).

The formation of the k_{II} phase in the former grains of β contributes to the enhancement of the aluminium segregation by depletion of this element in the adjacent areas of the Fe_3Al precipitates, so that, as can be seen from figure 2a, there is some tendency in their association

with the bainite plates (solid solution with a smaller degree of aluminium oversaturation than in the martensite α'_1).

The aluminium segregation is also found in the case of aluminium bronzes without iron additions, the cause being attributed to the transformation of the disordered β solution into an ordered solution, transformation that precedes the intermediate bainitic one. The ordered solid solution shows a higher concentration of aluminium and causes a decrease in this element ratio in the adjacent areas, respectively in the remaining β untransformed matrix, favoring the bainite germination [8].

In certain areas of the boundaries of the former β phase one can observe a mixture of phases made of solid solution (light coloured areas) and compound (dark coloured areas), the latter being most likely rich in Fe, namely phase k (fig. 2b).

There is also a slight changing in the morphology of the bright areas, from plate-like to rod-like, the latter being characteristic to the solid solution with an aluminium content close to the equilibrium one. These areas were most likely formed as a result of more significant diffusion phenomena at grain boundaries due to the excess of defects.

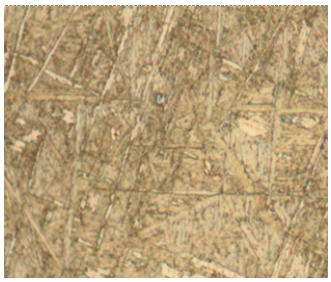

Fig. 2.a) Optical microstructure of B2 sample, x500, reagent: 25mL HCl + 5g $FeCl_3$ + 100mL H_2O

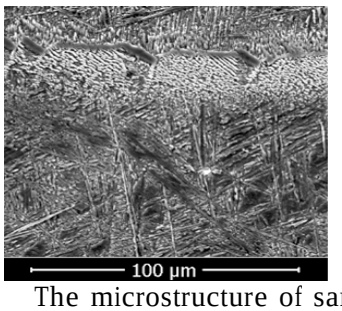

Fig. 2.b) Scanning electron micrograph of B2 sample, secondary electron image showing a mixture of martensite (dark-gray) and bainite (light coloured acicular zones)

The microstructure of sample B3 is similar to the microstructure of the quenched sample, barring the fact that dark areas attributed to martensite are narrower and bainite plates are much better highlighted, probably due to the trend of morphology changing from plate-like to rod-like.

This is due to the decrease of the degree of supersaturation in alloying elements of bainite, which initiates the precipitation of γ_2 and possibly k_V compounds. The transformation of martensite into α solid solution and γ_2 and k phases is much better observed at the grain boundary for sample B3 as compared to sample B2.

The microstructure of sample B4 (fig. 4) consists of α solid solution and γ_2 phase (possibly also k_V). The platiform/ needle-like aspect of the solid solution bright areas suggests its slight oversaturation due to the relatively low tempering temperature.

Figure 5 shows the microstructure of B5 sample, consisting of α solid solution and γ_2, possibly k_V phases. The α solid solution has an intermediate morphology, between the bainite specific flat plates and the rod-like rough one found in B1 sample. This indicates the existence of some degree of oversaturation.

Is has to be mentioned that k_{II} precipitates are found in all samples, regardless of the heat treatment. The optical micrographs also show their characteristic gray-blue color.

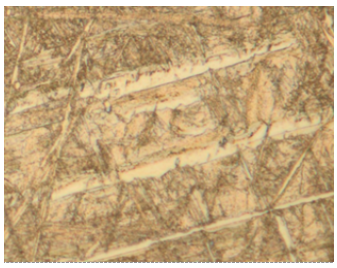

Fig. 3.a) Optical microstructure of B3 sample, x500, reagent: 25mL HCl + 5g $FeCl_3$ + 100mL H_2O

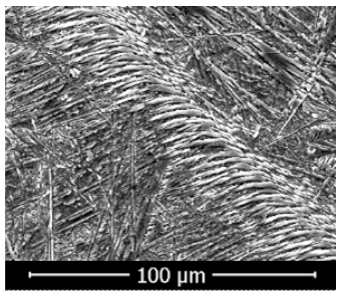

Fig. 3.b) Scanning electron micrograph of B3 sample, secondary electron image showing bainite, martensite and a mixture of α and compounds at grain boundaries

Fig. 4.a) Optical microstructure of B4 sample, x500, reagent: 25mL HCl + 5g $FeCl_3$ + 100mL H_2O

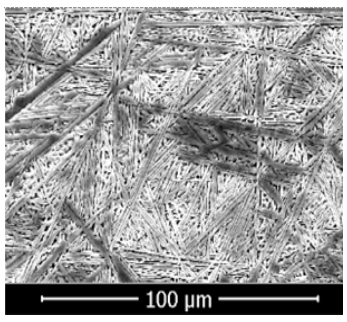

Fig. 4.b) Scanning electron micrograph of B4 sample, secondary electron image showing an α and γ_2 (possibly also k) mixture

Fig. 5.a) Optical microstructure of B5 sample, x500, reagent: 25mL HCl + 5g $FeCl_3$ + 100mL H_2O.

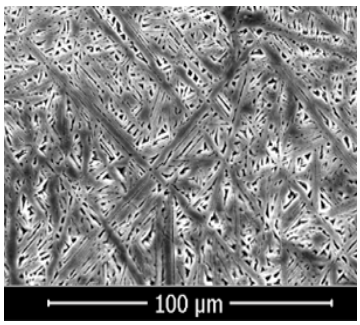

Fig. 5.b) Scanning electron micrograph of B5 sample, secondary electron image showing an α rod-like and γ_2 (possibly also **k**) mixture

The k_{IV} precipitates are present in the solid solution, finely dispersed, only in the annealed bronze. This is because the first type of precipitates is formed at high temperatures, starting at about 900-1000°C, in the β solid solution, and the second type is formed at lower temperatures in the proeutectoid solid solution. Therefore the formation and

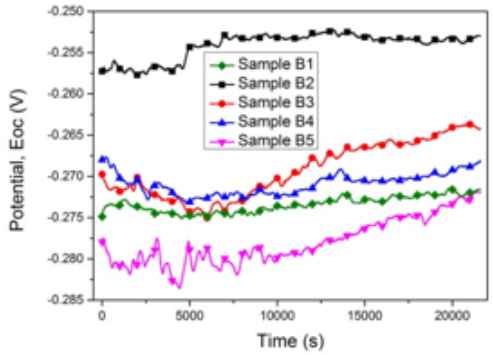

Fig.6. Open circuit potential E_{OC} *vs.* time for B1÷B5 samples

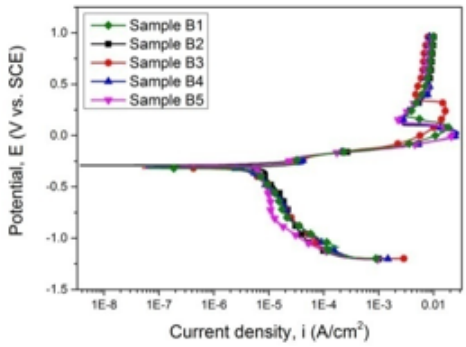

Fig.7. Potentiodynamic polarization curves for B1÷B5 samples

Sample	E_{oc} (mV)	E_{corr} (mV)	i_{corr} (μA/cm²)	β_c (mV)	β_a (mV)	Rp (kΩxcm²)	CR (mm/y)
Sample B1	-271	-306	4.93	114.05	99.55	4.68	0.111
Sample B2	-253	-282	7.76	160.80	99.23	3.43	0.174
Sample B3	-264	-301	6.85	129.41	105.40	3.68	0.154
Sample B4	-268	-306	5.34	100.49	105.92	4.19	0.120
Sample B5	-272	-304	4.61	118.84	98.36	5.07	0.103

Table 3
PARAMETERS OF THE ELECTROCHEMICAL CORROSION PROCESS

distribution of the k_{IV} precipitates are influenced by the cooling rate. Thus by heating for quenching at 900°C the k_{IV} phase is solubilized in the β matrix and subsequent cooling, carried out at high cooling rate, prevents its reprecipitation. Tempering heat treatments performed successively at subcritical temperatures of 200, 400 and 550°C lead to formation of the k_V dispersed phase in the α solid solution, because in quenched and tempered samples obviously no proeutectoid α phase is formed.

Electrochemical characterization

The variation of open circuit potentials (E_{oc}) corresponding to the tested samples is shown in figure 6, and the potentiodynamic polarization curves are shown in figure 7.

Table 3 shows the main parameters of the electrochemical corrosion process.

Considering the E_{OC} and E_{corr} potentials one may find that the five samples show close values, but the best behavior in a coupled system is that of sample B2 (negative potential, with the lowest value in modulus) followed by sample B3, while sample B5 is characterized by the lowest corrosion resistance (negative potential with the highest value in modulus).

The slightly cathodic nature of sample B2 relative to other samples can be ascribed to a predominantly monophasic (martensitic) structure with a rather uniform distribution of aluminium, without Cu_9Al_4 (γ_2) compound or **k** compounds being part of an eutectoid mixture or finely precipitated from martensite. They determine in the solid solution depleted micro-zones in the main alloying element. Samples B1 and B5 have similar structures, although their formation pattern is different: the main α phase, rod-like, and compounds γ_2 and **k**; in addition, a very small amount of martensite is also found in sample B1. In this context, they have roughly the same potential: -271 mV vs. -272 mV respectively.

The other electrochemical corrosion process parameters - current density i_{corr}, polarization resistance R_p and corrosion rate CR - characterize the pitting or crevice corrosion resistance which are corrosion types that do not involve the contact between two alloys immersed in the electrolyte.

Taking into account these parameters, one can estimate that the B5 sample has the best corrosion resistance, exhibiting the corrosion current lowest value, the polarization resistance highest value and the lowest corrosion rate as against sample B2 that is the less resistant to corrosion.

A corrosion resistance very close to that of sample B5 is showed by sample B1.

Sample B2 shows a structure composed of martensite (the main phase), needle-like microvolumes of α supersaturated phase (bainite) and Fe_3Al compounds. Martensite is anodic both with α solid solution and with Fe_3Al phase [9]. It is also an non-equilibrium phase, characterized by a higher level of internal stresses as compared to equilibrium phases. Under these conditions, sample B2 will have the weakest corrosion resistance.

Sample B3 quenched and tempered at 200°C has a similar structure to sample B2 but anodic areas with martensitic structure are smaller; thus the corrosion resistance is slightly improved (i_{corr} = 6.85 vs. 7.76 μA/cm², R_p = 3.68 vs. 3.43 kΩxcm², CR = 0.154 vs. 0.174 mm/y).

Samples B4 and B5 have a similar structure, consisting of white α crystals, γ_2 compounds and possibly k_V as well as k_{II} compounds. The latter are cathodic in relation to α, but do not significantly affect corrosion resistance because they are in a small amount. The γ_2 phase is the most prone to corrosion of all Cu-Al compounds [10] and all bronze phases (α, martensite and k-type compounds) [11].

The intensity of the corrosion phenomenon is closely related to its degree of dispersion in the solid solution α, as well as to the morphology of the solid solution (plate-like vs. rod-like).

Thus the mostly acicular aspect of α solution and dark coloured zones of compounds are to be noticed in sample B4. The latter has a lower corrosion resistance than B5 sample, where the α crystals show a close to rod-like morphology and the dark areas have a much higher discontinuity. Both B4 and B5 samples exhibit better corrosion resistance than B2 and B3 samples as a result of martensite decomposition on tempering as well as of stress relief phenomenon.

Sample B1 is rated as the best corrosion resistant after B5 sample on the one hand owing to the proeutectoid rod-like α phase and on the other hand due to the fact that the eutectoid phase with the highest corrosion susceptibility, γ_2, is discontinuous. This is a result of iron effect on grain refinement.

A less corrosion resistant B1 sample relative to B5 sample is determined by the existence in the bronze structure of both the eutectoid ($\alpha + \gamma_2$) and the martensite.

Conclusions

This paper presents several test results on the corrosion resistance in a saline medium of a bronze with 10.2% Al, 1.32% Fe and 1.21% Mn submitted to the following heat treatments: annealing at 900°C /furnace cooling (sample B1), quenching at 900°C/water cooling (sample B2), quenching at 900°C/water cooling followed by tempering at 200, 400, and 550°C, respectively (samples B3, B4 and B5).

Prior to perform the corrosion tests, the five samples were investigated by optical and scanning electron microscopy.

After establishing the correlation between the structural characteristics of the heat treated samples and the results of the corrosion tests, one can conclude the following:

All five samples show close values of open circuit potentials (E_{OC}) and corrosion potential (E_{corr});

The most resistant sample on galvanic corrosion is B2 sample, and the most anodic sample with respect to the other is B5; the cathodic character of B2 sample is most probably due to a structure made of the prevalent martensite and bainite, with a relatively uniform distribution of aluminium; a lower corrosion resistance is showed by the tempered structure made of α solid solution and γ_2 and k compounds (B5 sample);

As for evaluation of corrosion resistance that do not involve the contact between two metallic materials immersed in electrolyte, the best behavior was found on B5 sample, followed by B1, B4, B3 and B2 samples;

The structure showing the best corrosion resistance is made of rod-like solid solution α and discontinuous γ_2/k compounds (B5 sample) as against to the weakest corrosion resistant structure consisting of martensite and bainite (α solid solution resulting from the massive transformation of the β - Cu_3Al - phase).

Reference

1.MATIJEVIC, B., SUSHMA, T.S.K., PRATHVI, B.K., Tehnieki glasnik, **11**, no.3, 2017, p. 107.

2.POWELL, C., WEBSTER, P., Copper Alloys for Marine Environments, Copper Development Association, CDA Publication no. 206, 2011.

3.NEJNERU, C., PERJU, M.C., SANDU, A.V., AXINTE, M., QUARANTA, M., SANDU, I., COSTEA, M., ABDULLAH, M.M.A.B., Rev.Chim. (Bucharest), **67**, no. 6, 2016, p. 1191.

4.HOWELL, P.R., On the phases, microconstituents and microstructures in nickel aluminium bronzes-technical report, Copper Development Association, 1997.

5.SLAMA, P., DLOUHY, J., KOVER, M., Mater. Tehnol., **48**, 4, 2014, p. 599

6.LABANOWSKI, J., OLKOWSKI, T., Archives of Foundry Engineering, **14**, no.2, 2014, p. 73.

7.*** Copper Development Association. Equilibrium Diagrams-Selected Copper Alloy Diagrams Illustrating the Major Types of Phase Transformations, no. 94, 1992, p.19.

8.GARWOOD, R.D., Special Report 93, Proc. Joint Conference of British Iron and Steel Association and The Iron and Steel Insitute, Scarborough, UK, May 1965.

9.LORIMER, G.W., HASAN F., IQBAL J., RIDLEY N., Brit. Corros. J., **21**, no. 4, 1986, p. 244.

10.BREACHA, C.D., LEEB, T.K., Proc. 12th International Conference on Electronic Packaging Technology and High Density Packaging, Shanghai, China, 2011.

11.MEIGH, H., Cast and Wrought Aluminium Bronzes-Properties, Processes and Structure, 2, Maney Publishing, Leeds, UK, 2000, p.111.

Manuscript received: 6.12.2017